

Articulated Object Reconstruction and Markerless Motion Capture from Depth Video

Yuri Pekelný and Craig Gotsman

Center for Graphics and Geometric Computing
Technion, Israel

Abstract

We present an algorithm for acquiring the 3D surface geometry and motion of a dynamic piecewise-rigid object using a single depth video camera. The algorithm identifies and tracks the rigid components in each frame, while accumulating the geometric information acquired over time, possibly from different viewpoints. The algorithm also reconstructs the dynamic skeleton of the object, thus can be used for markerless motion capture. The acquired model can then be animated to novel poses. We show the results of the algorithm applied to synthetic and real depth video.

Categories and Subject Descriptors (according to ACM CCS): I.3.5 [Computer Graphics]: Computational Geometry and Object Modeling I.3.7 [Computer Graphics]: Three-Dimensional Graphics and Realism

1. Introduction

Traditional 3D scanning applications involve only static subjects, and the main challenge in these applications is to produce an accurate digital model of the scene geometry. Over the past decade, a multitude of algorithms have been proposed to address this problem, and by now it may be considered (almost) solved. Thus attention is shifting to dealing with dynamic scenes, i.e. ones in which the subjects are moving.

Since the scene is dynamic, at first glance it may seem that the problem is not well-defined. What does scanning a scene in which the geometry is constantly changing mean? What do we expect as the output of this process? The problem is compounded by the fact that in order to capture any motion accurately, we must sense the scene at real-time rates, a technological challenge for the scanning device in its own right.

To address the last challenge first, it seems that the most suitable sensor to use for dynamic scenes is the so-called *depth video camera*. Such a camera provides an image of the scene, where each pixel contains not only traditional intensity information, but also the geometric distance from the camera to the subject at that pixel. A number of commercial cameras generating this information at video rates have appeared over recent years [CVCM, 3DV, PS, VZS], and the state-of-the-art of the technologies involved is improving rapidly. Prices are also dropping, so we expect that depth video cameras will be available at reasonable cost within the next few years.

The simplest version of the dynamic scene scanning problem is motion capture of a piecewise-rigid 3D subject (such as a person). This means that as output we are not interested

in the precise geometry of the subject, rather in the rough motion of a “skeleton” representing its rigid parts, of which there are usually just a few. Motion capture is performed today using elaborate rigs involving markers placed on the subject, and it would be useful to have a device capable of markerless motion capture based only on depth cameras. This is the objective of a number of commercial companies [3DV,PS] who are developing depth cameras for use as motion capture and gesture recognition devices in interactive consumer-level gaming applications.

A more challenging version of the problem is full 3D scanning of dynamic piecewise-rigid 3D objects. The desired output is not just a skeletal model of the subject, rather a complete 3D model of the surface of each of the rigid components, and a description of the motion of each such component over time. It would be ideal if all this could be computed in real time, but even offline computation would be useful for many applications, especially those in which it is impossible to prevent the subject from moving during the scanning process.

The most challenging version of the problem is when the objects in the scene are deforming over time in a non-rigid manner. Here the description of the object motion is more complicated, possibly even non-parametric.

This paper addresses the second question: scanning a piecewise-rigid subject. The goal of the algorithm is to recover the skeletal motion of the subject and to reconstruct its surface geometry from a sequence of range images captured by a *single* (possibly moving) depth camera. The main issues are identification and tracking of the rigid components and reconstructing their surfaces despite partial occlusions present in each frame.

Since the system is markerless, it has no easily available correspondence information between points in different frames, thus it does not know which rigid component each sampled point (pixel) belongs to, nor does it know the rigid motion of any component between frames or the relative (rigid) camera transformation between frames. However, the temporal sampling rate is assumed to be sufficiently high, so that the relative position of each rigid component between each two consecutive frames is close enough to provide a good initial estimate for the classical Iterated Closest Point (ICP) registration algorithm.

2. Previous Work

There are several algorithms in the literature for markerless motion capture from traditional video. Many of them [MCA06, CBK03, TAM04] recover articulated object motion from visual hull sequences, acquired from object silhouettes. These algorithms require multiple synchronized video cameras observing the subject from several different directions, which incurs complications related to temporal and spatial multi-camera calibration.

There are also several model-based approaches [GWK05, RAPK06, BKM*04] capable of recovering articulated object pose from a single depth image by fitting it to a model. This, however, requires a very detailed and calibrated model in order that a single depth image suffice.

The algorithm proposed in [AKP*04] recovers a full 3D model of the subject in addition to pose detection. This algorithm also does not require markers, but each input pose must be a complete surface mesh. Hence this algorithm is inapplicable to depth video input.

We also aim to reconstruct a full 3D model of the subject. To register multiple components of an articulated subject, we assume a piecewise-rigid skeletal structure. A different approach was proposed in [MFO*07]. It overcomes the registration problem by splitting the input data into small almost-rigid pieces. This algorithm assumes dense spatial and temporal sampling and performs the registration using kinematic properties of the space-time surface. An articulated version of this may be possible.

Several authors have proposed algorithms which recover both the subject geometry and its motion. For example [AFW*99] proposes an algorithm for articulated model reconstruction. However the algorithm uses a pairwise frame registration approach, hence becomes very inefficient when applied to a long input data sequence. The authors also admit that the pairwise registration, as opposed to a more global approach, leads to suboptimal results.

The authors of [KVD06] propose a model-based human body motion tracking system called VooDoo. This system models the human body as a collection of ten moving rigid cylinders (organized hierarchically), and tracks their movement through time using the ICP registration algorithm. It is necessary to manually resize the model for each different human subject. VooDoo fails to give good results using depth data input alone and requires additional data from 2D tracking sensors to achieve good results.

Another recent work [WJH*07] addresses a similar problem, but with a deformable subject. It performs iterative reconstruction and optimization of the 4D structure assuming spatio-temporal smoothness. However the algorithm is computationally heavy and it is not clear if it is capable of reconstructing a complete 3D model of a deformable object from depth video.

To the best of our knowledge, ours is the first method capable of reconstructing a *complete* 3D model of an articulate object using a *single* depth video camera. This is also the first *markerless* motion capture algorithm that does not require a template *mesh* of the subject.

3. The Algorithm

3.1. Assumptions and outline

An articulated object consists of a set of connected rigid components. It is customary to refer to the rigid components as “bones”, and to the connection between two bones as a “joint”. The actual 3D geometry of the surface associated with the bone is called a “skin”. We make the following assumptions on the input:

1. The motion of the subject is piecewise-rigid.
2. The combinatorial structure of the skeleton of the subject is known, i.e. n - the number of bones in the subject - is given, and we are given a list of ID pairs of connected bones.
3. All bones are (at least partially) visible in the first frame, and a rough assignment (segmentation) of image points to bones is given for this frame (see Fig. 1).
4. During acquisition, the subject moves in such a way that most of its surface points are visible to the camera at some point in time.

Note that the information we assume about the skeleton is purely combinatorial as opposed to geometric, namely, we do not know anything about the length of bones or the positions of joints. First frame segmentation is acquired by a manual “coloring” process.

The algorithm tracks each bone of the subject almost independently throughout the sequence. Each image point is assigned a “bone index” – an integer in the set $\{0, \dots, n\}$. The index 0 indicates that the point’s bone index is undecided, i.e. we have not been able to determine which bone the image point belongs to with sufficient confidence. These undecided points are typically in the vicinity of joints (where more than one bone competes for that point). The first objective is to accumulate over time the skin geometry of each bone. The second objective is to track in some global coordinate system the motion of each bone over time.

The algorithm runs in several independent stages on each depth image of the sequence. For each new image the algorithm finds the new pose of each rigid bone by registering the accumulated skin geometry of the bone to the new image points. The correctness of the registration is verified by computing the coordinates of the joints of the skeleton and checking that the skeleton remains connected after apply-

ing the new transformations. The new image points are then segmented into bones, namely a bone index is assigned to each image point. A subset of these new points covering regions previously not sampled are then added to the accumulated skins. The following sections describe each stage of the algorithm in detail and elaborate on the relations between them. Fig. 3 summarizes the algorithm.

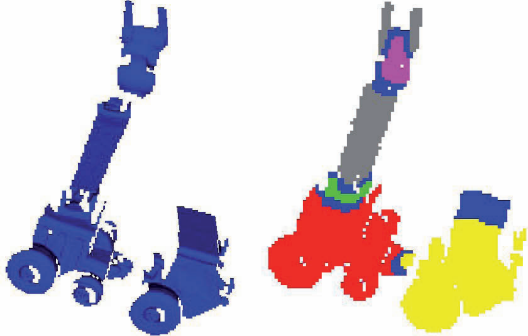


Figure 1: Rough user segmentation of the first frame of the real-world “Tow Truck” depth video sequence to bones by painting the image pixels (**left**) with different colors (**right**). Blue in right image means undecided bone index.

3.2. Depth image preprocessing

Several components of our algorithm require normal vectors of the input data points. To compute the normals we construct a simple mesh from the depth image points (pixels) and calculate the normals at vertices by area-weighted average of the normals to neighboring faces. This is a simple method which gives reasonable results if the data is not too noisy. A more robust estimate could use the normal to a least squares plane approximating a few neighboring points, but this requires more computation. To construct a simple mesh we use the rectilinear structure of the image grid. We generate all vertical, horizontal and the shorter diagonal edges, while ignoring those whose length is larger than four times the grid size. After that we form triangles. This process also filters out single points which are farther than one grid unit from the scanned point cloud, which are considered outliers.

3.3. Finding bone transformations

The algorithm processes each input frame separately in chronological order. Each frame is analyzed based on the results from the previous frames. During this process the algorithm maintains two global data structures. One is the accumulated 3D point clouds of the skins (each bone is accumulated separately). The other is the set of all rigid bone transformations from the first frame to all other frames. From this set of transformations we can find the relative transformation of any bone between any two frames.

To find the relative rigid bone transformation for each bone to a new input frame t , we register the skin of that bone, accumulated so far, to the points of frame t using the Iterated Closest Point (ICP) registration algorithm [BM92] (note that we do not register in the opposite direction). We use the bone’s transformation from the first frame (where the reconstructed skin is accumulated) to frame $t-1$ as the initial transformation for the ICP process. If the sampling rate is dense enough this is an excellent choice. The bones are registered in a hierarchical order, recursing (with BFS) through the skeletal structure, starting from the root bone.

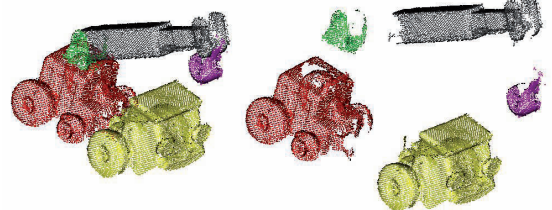


Figure 2: Skin geometry. 3D points are accumulated for each bone separately (**right**). Each of these is later meshed separately using a point cloud meshing algorithm.

There are several cases where the ICP registration may fail. For example, when the bone is occluded in the new frame or when the overlap between the skin and the points in the new frame is small. Our algorithm treats both cases as occlusion and provides a number of methods of detecting and recovering from ICP failure. For each bone we start by trying to find the rigid transformation using ICP without any additional constraints. If we fail, we find the joint locations between the current bone and all other bones connected to it and repeat the ICP process together with the joint constraint (see Section 3.6). If we fail again, the bone is considered occluded and we approximate its transformation using skeleton structure constraints, as described in Section 3.4.

The ICP algorithm is known to be sensitive to outliers. To detect such outliers, we employ a number of heuristics, similar to [RHHL02]. Corresponding pairs of points (identified as such by the ICP nearest neighbor pairing) of the following types are deemed outliers, hence ignored.

1. Pairs whose distance from each other is larger than a threshold.
2. Pairs whose angle between normals is larger than a threshold.
3. Pairs whose target point lies on the input mesh boundary.

To make the ICP algorithm more robust and accurate, we use dynamic thresholds for items 1) and 2). The initial distance threshold is 15x the image grid size and it decreases to 3x that after 5 iterations. The initial angle threshold is 80°, decreasing to 20° after 4 iterations.

3.4. Treating occlusion

As mentioned above, we call a bone *occluded* if the ICP registration algorithm failed. We have several ways to detect when the registration fails:

1. The number of corresponding ICP point pairs falls below a threshold.
2. The ICP algorithm does not converge quickly.
3. The resulting transformation does not satisfy the constraint connecting this bone with its parent bone, namely, the distance between current bone joint transformed with the current bone transformation and the same joint transformed with the connected bone transformation is larger than a threshold.

Even if the bone is occluded, we would like to find an approximate transformation that satisfies the skeleton joint constraints, to keep the reconstructed skins connected. We find an approximate transformation of the occluded bone based on the transformations of the neighboring bones and skeleton joints constraints:

1. If the occluded bone is connected to just one bone, apply this neighbor's relative transformation to the occluded bone in the frame in which it is occluded.
2. If the occluded bone is connected to two bones, use the rigid transformation that best fits both joint's movements and minimizes the relative rotation between the bones.
3. If the occluded bone is connected to more than two bones, approximate its transformation by finding the rigid transformation that best fits all joints movement.

3.5. Bone assignment

Once we have found the relative transformation of all bones between the first frame and a new frame t , we need to segment the points in the new frame into bones. This implies for each point, once segmented, a set of rigid transformations from frame t to all previous frames $1..t-1$.

If the point p belongs to the skin of a bone b , then the rigid transformation of b should translate p to the neighborhood of b 's skin. To determine which bone p best belongs to, we apply all possible bone transformations (computed in the previous step) to p and calculate the *distance* between the result and the nearest point of b 's skin: $d_b(p) = (1-\alpha)d_n(p)+\alpha d(p)$ (typically $\alpha=0.1$), where $d_n(p)$ is the distance from p to the tangent plane at $\text{nearest}(p)$ – the local approximation of the reconstructed surface, and $d(p)$ is the distance from p to $\text{nearest}(p)$. The purpose of the second term is to reject far points that fall near the tangent plane.

To decide which bone the point p belongs to among all candidates, we use the following confidence measure:

$$C_b(p) = \frac{1}{d_b(p)} / \sum_{b' \in \text{bones}} \frac{1}{d_{b'}(p)},$$

Note that

$$\sum_b C_b(p) = 1$$

After calculating confidences for all possible bone assignments we find b_{max} – the bone index which maximizes $C_b(p)$. This is just the bone index which minimizes $d_b(p)$. However, we rely on this only if its confidence is significantly larger than the confidences of the other bones, namely, if $C_{b_{max}}(p) > \tau$ (typically $\tau=0.8$) and $d_{b_{max}}(p) < \text{sampling density}$, then we assign p to b_{max} . Otherwise p 's bone index remains undecided ($=0$) and the point does not contribute to skin geometry and future ICP registrations.

As mentioned in the previous section, some bones may be occluded, thus their transformations are only an approximation based on skeleton connectivity constraints. To avoid accumulating error due to these approximations, we consider as candidates only bones that are not occluded.

3.6. Tracking the skeleton

A joint point u is a point connecting two bones b_1 and b_2 . Therefore transforming u from the first frame to any other frame t with both bone transformations T_1 and T_2 should give the same result: $T_1(u) = T_2(u)$. We seek a joint u that satisfies this property for transformations to all frames $2..t$. Therefore, following [AKP*04], for each pair of connected bones b_1 and b_2 we solve the following minimization problem for u :

$$u = \arg \min \sum_{i=1}^t \|T_{b_1}^i(u) - T_{b_2}^i(u)\|^2 + \gamma \|u - c\|^2$$

where T_b^i is the transformation of bone b in frame i . c is the centroid of a set of points in the vicinity of the joint, namely, a small set of points of b_1 close to b_2 and vice versa, in the first frame. Typically $\gamma=0.1$. The second term stabilizes the solution in the cases where the first term admits more than one possible solution. As before, we ignore all transformation pairs that contain approximate transformations for occluded bones.

To complete the skeleton construction we choose the bone with the largest number of points in the first frame to be the root bone and connect all other bones in a hierarchical order.

3.7. Accumulating skin geometry

To reconstruct the skin geometry of a bone, we combine the depth samples from different frames by registering them in the coordinate system and the subject pose of the first frame. This results in a set of points (and their normals) accumulated for each bone. The skin geometry may then be reconstructed from this data, bone by bone, by any point cloud meshing algorithm (e.g. [KBH06, ACS*07]). See Fig. 2.

To register some point p from frame t into the coordinate system of the first frame, we need to know p 's bone index and the rigid transformation of the bone between this and the first frame. At each stage of the algorithm, when we obtain this information for a point, it may contribute to the reconstructed 3D model by applying the transformations. To reduce redundancy, thus limit the number of points in the reconstruction without compromising the skin com-

pleness, we adopt only new points which are not too close to the set of points accumulated so far. As each sample point supposedly originates at the subject surface, our measure of the proximity of a point p with existing points on the subject is the distance from p to the nearest point in the dataset – $\text{nearest}(p)$ – projected onto the tangent plane of $\text{nearest}(p)$. We add a new point to the skin geometry only if this distance is larger than a threshold - typically half the grid size. Lowering this threshold will increase the number of points contributing to the surface model, but also increase the algorithm runtime. The more frames sampled from different viewpoints, the more complete the reconstructed geometry becomes.

In practice, assignment of image points to the individual skins is done only after *all* bones have been identified in the image, as described in Section 3.5. The segmentation process does not assign a bone index to every single point - the points whose bone cannot be determined with high confidence are left “undecided” and do not contribute to the accumulated skin geometry.

1. Obtain from the user a rough segmentation of the first frame and the skeleton connectivity information
2. For $t = 1..T$ do:
 - 2.1. Calculate point normals and detect boundary points (Section 3.2)
 - 2.2. Find a relative transformation for each bone in the reconstructed model to the new frame t (Section 3.3)
 - 2.3. Based on the transformations and the new frame data, detect points with suspect bone assignments in the reconstructed model and remove them (Section 3.8)
 - 2.4. Assign bone indices to points in the new frame t (Section 3.5)
 - 2.5. Find joint locations based on all bone transformations from frame 1 to frames $2..t$ (Section 3.6)
 - 2.6. Add points from frame t to regions of the skins not yet covered (Section 3.7)
3. Apply meshing algorithm to the accumulated skin of each bone (e.g. [KBH06])

Figure 3: The reconstruction algorithm.

3.8. Filtering skin geometry

Bone skins are reconstructed by accumulating 3D points which are assigned to bones that provide the best registration for them (as described in Section 3.5). When two bones have similar transformations, it may be hard to determine which bone is a better match. An erroneous assignment may compound later in the process. To prevent this we try to

identify points assigned incorrectly and remove them retroactively from the skins based on the information in each new frame.

First we apply the bone transformations from the first frame to the current frame for non-occluded bones. Then we check each pair of connected (and unoccluded) bones to see if they contain points representing two parallel surfaces. More precisely, we look for pairs of points p from b_1 and $\text{nearest}(p)$ from the neighbor b_2 , whose distance projected on the tangent plane of $\text{nearest}(p)$ is shorter than the distance projected along the normal direction of $\text{nearest}(p)$. All points satisfying this condition are removed from the skin.

4. Experimental Results

4.1. Test cases

We have implemented our algorithm and applied it to both real-world and synthetic depth video sequences.

Real data was captured by a Vialux Z-Snapper depth camera (based on structured light technology) [VZS] for two physical models: a toy robot and a toy tow truck, consisting of 7 and 5 bones respectively. Both motion sequences contain 90 frames, captured from arbitrary viewpoints while the model was animated. The results are shown in Figs. 6 and 7. The top row contains a subset of the input depth video sequence. Since structured light scanning technology is based on illuminating the subject from an angle slightly different than that of the camera, there are occlusions due to “self-shadows” from the illumination angle, which can be quite significant at short ranges. The second row shows the segmentation of the depth images to no more than the number of components (“bones”) specified by the user in the first frame. The third row shows the accumulated bone skins in one static model in the same poses as captured in the sequence, after our processing. Due to occlusions in the input, or undecided classification of image points, there are still surface regions where data is missing, resulting in some holes. The fourth row shows the same poses after the bone geometries were meshed (as point clouds) to closed manifold surfaces (each bone separately) using the algorithm of [KBH06] (kindly provided by the authors). The results are quite good despite the noise and occlusions in the depth images.

While our algorithm is designed for subjects whose motion is piecewise-rigid, it is also applicable as an approximation of the motion of deformable subjects in some cases. Significant examples are models of skinned articulated bodies, such as human and animals. We tested this on a synthetic sequence (180 frames) of an articulated model of a Beast containing 12 bones. The motion sequences for this model were a variation on the motion taken from the CMU Graphics Lab Motion Capture Database [CMU]. The inputs to our algorithm were the captured Z-buffers of the rendered animations.

The results on this synthetic deformable model are depicted in Fig. 8. As expected, since the motion is not truly piecewise-rigid, the results were not perfect. The segmentation procedure, which feeds the rest of the process, did not always classify the image points correctly. An example is the rear end of the subject (colored light blue in the figure) which was classified as part of the upper right leg instead of the torso (colored purple). This led to artifacts in the reconstruction, where that rear end sometimes protrudes, giving the impression of a “tail”.

4.2. Performance

Our algorithm was implemented in MATLAB, and tested on a 2.8GHz Pentium D with 1GB of RAM. It was not seriously optimized for performance. With an efficient implementation, better hardware and some algorithm improvements, we are confident that our algorithm can be significantly accelerated, within range of real-time performance, as other ICP-based reconstruction algorithms [RHHL02]. The only part of our algorithm that we did optimize was finding nearest neighbors among points in 3D, since the algorithm spends a significant part of its runtime on these types of operations during ICP. We used the ANN C++ library [MA06], and yet still 63% of the runtime is spent on nearest neighbor searching. Table 1 gives the performance summary for our three test sequences. The times quoted there do not include the preprocessed normal computations.

4.3 The video

The video accompanying this paper demonstrates the different stages of our scanning and motion capture procedure and shows some new animation sequences that may be generated once the dynamic object is scanned. The video may be found at www.cs.technion.ac.il/~gotsman/mocap.mov

Model	#bones	#frames	points /frame (average)	average time/frame (sec)
Truck	5	90	5,349	1.68
Robot	7	90	9,338	4.41
Beast	12	180	4,204	2.50

Table 1: Algorithm runtime performance.

4.4 Limitations

A key component of our algorithm is the ability to detect whether the inter-frame ICP registration succeeded or not. This detection prevents incorrect segmentation, which could be damaging. For some types of structured data, this detection mechanism fails. For instance, the model of a deforming human hand (see left part of Fig. 4). The cylindrical symmetry of the fingers confuses the ICP because there are many seemingly valid, but wrong, registrations. So even if the camera rotates 360° around a finger, the parts of the finger visible in each frame will always be registered to each other in one region of the finger, instead of completing

the entire finger circumference. Consequently, we generate both incorrect motion capture and an incorrect 3D skin.

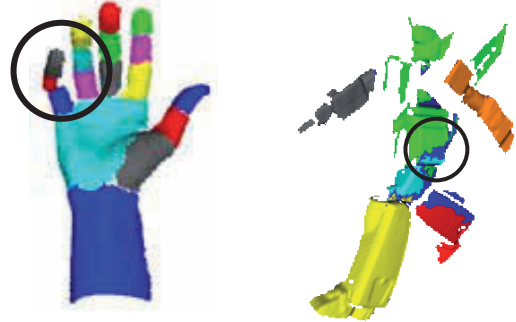


Figure 4: (right) ICP failure to register a bone, due to cylindrical symmetry of the bone. The red skin remains incomplete. (left) Incorrect segmentation (of the light blue and green points inside the black circle) due to “sliding planes”.

Another problem we encountered is incorrect segmentation in the case of two “sliding” parallel planes. For example, the left leg of the “Robot” model (colored in light blue in the right part of Fig. 4) can only move parallel to the left side of the robot’s body (colored in green). In the marked region, the upper light blue points were mistakenly assigned to the leg and the lower green points were mistakenly assigned to the body. The reason for this is that when we have two small transformations perpendicular to the plane normal, both transformations align the points of one plane very close to other points of that plane. If one of these transformations brings the point to an unscanned region of that plane, the algorithm may incorrectly conclude that the other transformation is the best one for this point.

4.5 Sensitivity to noise

In Section 4.2 we showed that our algorithm is capable of reconstructing a full 3D object from real-world data without any noise reduction. However, some depth video cameras are more noisy than others, especially those operating at high resolutions and frame rates, thus it is important to know how robust our algorithm is to noisy inputs. We tested this by adding Gaussian noise to the depth channel of the synthetic “Beast” sequence. Our results show that the component of the algorithm which is most sensitive to noise is detection of registration correctness. Adding noise to the input without calibrating the algorithm thresholds results in many false alarms – supposed registration failures in cases when the transformation was actually correct. For example, when the original depth image of the first input frame was contaminated with noise of SNR 23db, the reconstructed model had a bump in the upper part of its right hand. The rest of the shape and the joint locations were reconstructed correctly. The relative Hausdorff distance between the two (as measured by the Metro tool) was 5% of the bounding box diagonal.

5. Summary and Conclusion

We have presented an algorithm capable of reconstructing a full 3D model of a dynamic articulated subject from a sequence of depth images taken by a single depth video camera. The algorithm segments the input set of point clouds to rigid components, detects rigid motions between the frames and reconstructs an articulated 3D model in a single pass over the data. Another pass may be performed in order to improve the joints consistency during motion. The algorithm detects bone occlusion and approximates skeleton-consistent motion for these occluded bones. In addition to 3D scanning, our algorithm tracks the skeleton of the subject, thus can be used for markerless motion capture over long sequences.

The Achilles heel of our algorithm is the requirement of manual segmentation of the first frame and specification of the combinatorial skeleton connectivity. We believe that both these components can potentially be automated using the approach described in [YP06] for automatic learning of articulated object structure.

Future versions of this work will improve the approximation in the case of a deforming subject which is not truly piecewise-rigid. In the performance domain, our implementation currently runs offline after the data has been captured. The holy grail is, of course, to optimize the performance of the system so that it may run in real-time. This will enable a variety of important applications in the entertainment world.

Acknowledgements

Thanks to David Mount and Sunil Arya for making available the ANN software package and to Michael Kazhdan for making available his software for 3D reconstruction from point clouds.

This research was partially funded by European FP6 IST NoE grant 506766 (AIM@SHAPE), the Israel Ministry of Science, the State of Lower-Saxony and the Volkswagen Foundation, Hannover, Germany.

References

- [3DV] <http://www.3dvsystems.com>
- [ACS*07] ALLIEZ P., COHEN-STEINER D., TONG Y., DESBRUN M.: Voronoi-based variational reconstruction of unoriented point sets. *Proc. Eurographics Symp. on Geometry Processing*. (2007), pp. 39–48.
- [AFW*99] ASHBROOK A. P., FISHER R. B., WERGHI N., ROBERTSON C.: Construction of articulated models from range data. *Proc. BMVC* (1999), pp. 183–192.
- [AKP*04] ANGUELOV D., KOLLER D., PANG H., SRINIVASAN P., THRUN S.: Recovering articulated object models from 3D range data. *Proc. Conference on Uncertainty in Artificial Intelligence* (2004), pp. 18–26.
- [BKM*04] BRAY M., KOLLER-MEIER E., MÜLLER P., VAN GOOL L., SCHRAUDOLPH N.N.: 3D hand tracking by rapid stochastic gradient descent using a skinning model. In *CVMP* (2004), pp. 59–68.
- [BM92] BESL P. J., MCKAY N. D.: A method for registration of 3D shapes. *IEEE PAMI*, 14:239–256, 1992.
- [CBK03] CHEUNG G., BAKER S., KANADE T.: Shape-from-silhouette for articulated objects and its use for human body kinematics estimation and motion capture. *Proc. CVPR* (2003), pp. 77–84.
- [CMU] CMU Graphics Lab Motion Capture Database, <http://mocap.cs.cmu.edu>
- [CVCM] <http://www.canesta.com>
- [GWK05] GREST D., WOETZEL J., KOCH R.: Nonlinear body pose estimation from depth images. *Proc. of DAGM* (2005), pp. 285–292.
- [KBH06] KAZHDAN M., BOLITHO M., HOPPE H.: Poisson surface reconstruction. *Proc. Eurographics Symp. on Geometry Processing*. (2006), pp. 61–70.
- [KVD06] KNOOP S., VACEK S., DILLMANN, R.: Sensor fusion for 3D human body tracking with an articulated 3D body model. *Proc. IEEE Conf. on Robotics and Automation* (2006), pp. 1686–1691.
- [MA06] MOUNT D. M., ARYA S.: ANN: A library for approximate nearest neighbor searching. Version 1.1.1, 2006, <http://www.cs.umd.edu/~mount/ANN/>
- [MCA06] MÜNDERMANN L., CORAZZA S., ANDRIACCHI T.: Markerless human motion capture through visual hull and articulated ICP, *Proc. NIPS Workshop* 2006.
- [MFO*07] MITRA N. J., FLORY S., OVSJANIKOV M., GELFAND N., GUIBAS L., POTTMANN H.: Dynamic geometry registration. *Proc. Eurographics Symp. on Geometry Processing* (2007), pp. 173–182.
- [PS] <http://www.primesense.com>
- [RAPK06] RODGERS J., ANGUELOV D., PANG H.-C., KOLLER D.: Object pose detection in range scan data. *Proc. CVPR* (2006), pp. 2445–2452.
- [RHHL02] RUSINKIEWICZ S., HALL-HOLT O., LEVOY M.: Real-time 3D model acquisition. *Proc. SIGGRAPH* 21, 3 (2002), pp. 438–446.
- [TAM04] THEOBALT C., DE AGUILAR E., MAGNOR M., THEISEL H., SEIDEL H.-P.: Marker-free kinematic skeleton estimation from sequences of volume data. *Proc. ACM VRST* (2004), pp. 57–64.
- [VZS] <http://www.vialux.de>
- [WJH*07] WAND M., JENKE P., HUANG Q., BOKELOH M., GUIBAS L., SCHILLING A.: Reconstruction of deforming geometry from time-varying point clouds. *Proc. Symp. on Geometry Processing* (2007), pp. 49–58.
- [YP06] YAN J., POLLEFEYS M.: Automatic kinematic chain building from feature trajectories of articulated objects. *Proc. CVPR* (2006), pp. 712–719.

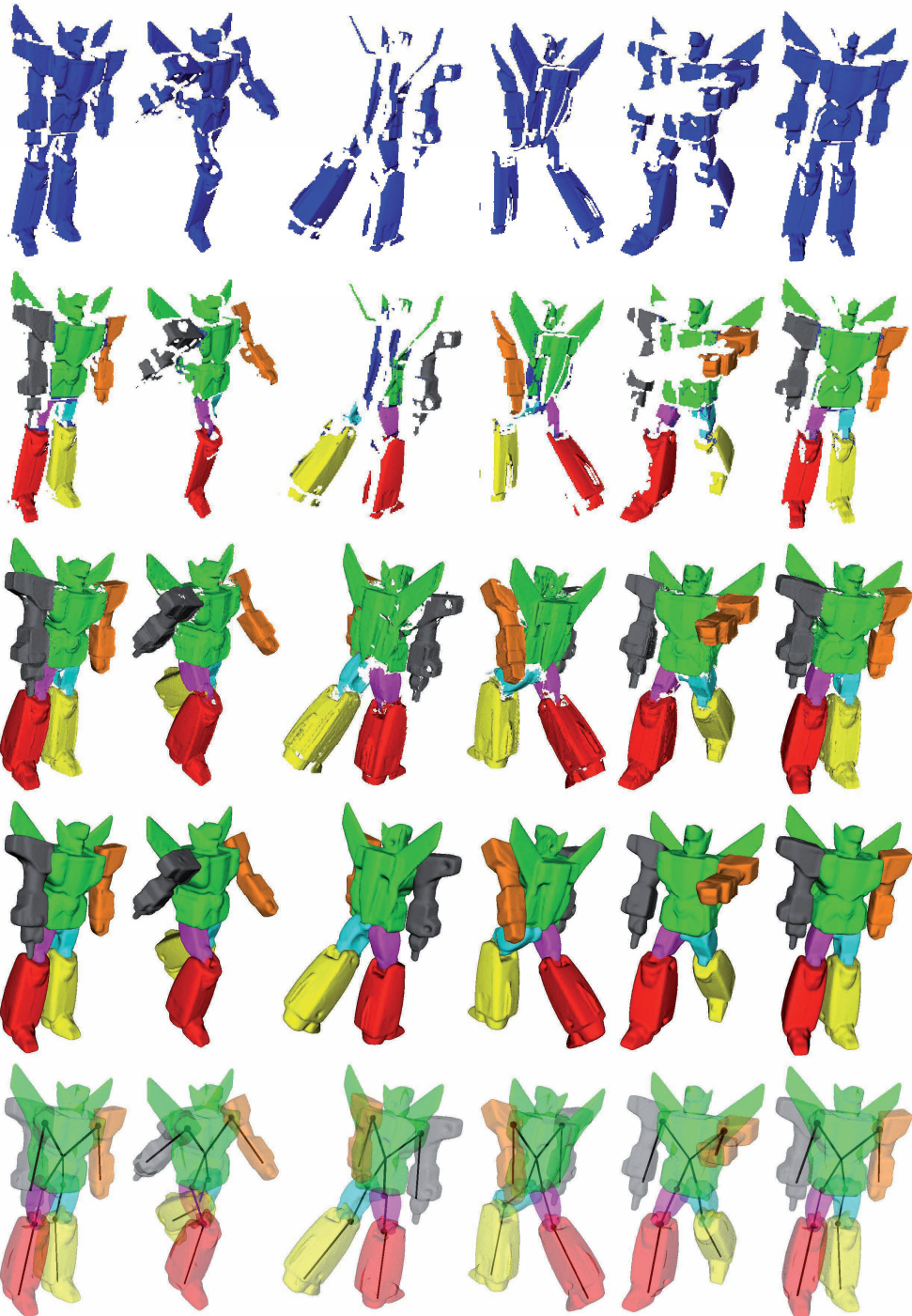


Figure 6: Scanning the dynamic real-world Robot model containing 7 bones: **(Top row)** Some of the input depth frames obtained by a Vialux depth video camera. Note the different camera viewpoints and model poses. **(Second row)** Segmentation of the input frames into bones. Dark blue regions are undecided. **(Third row)** Accumulated skin geometry in input poses. Holes are present where the surface was occluded in all input frames. **(Fourth row)** Complete model in input poses after skin reconstruction. **(Bottom row)** Reconstructed skeletons.

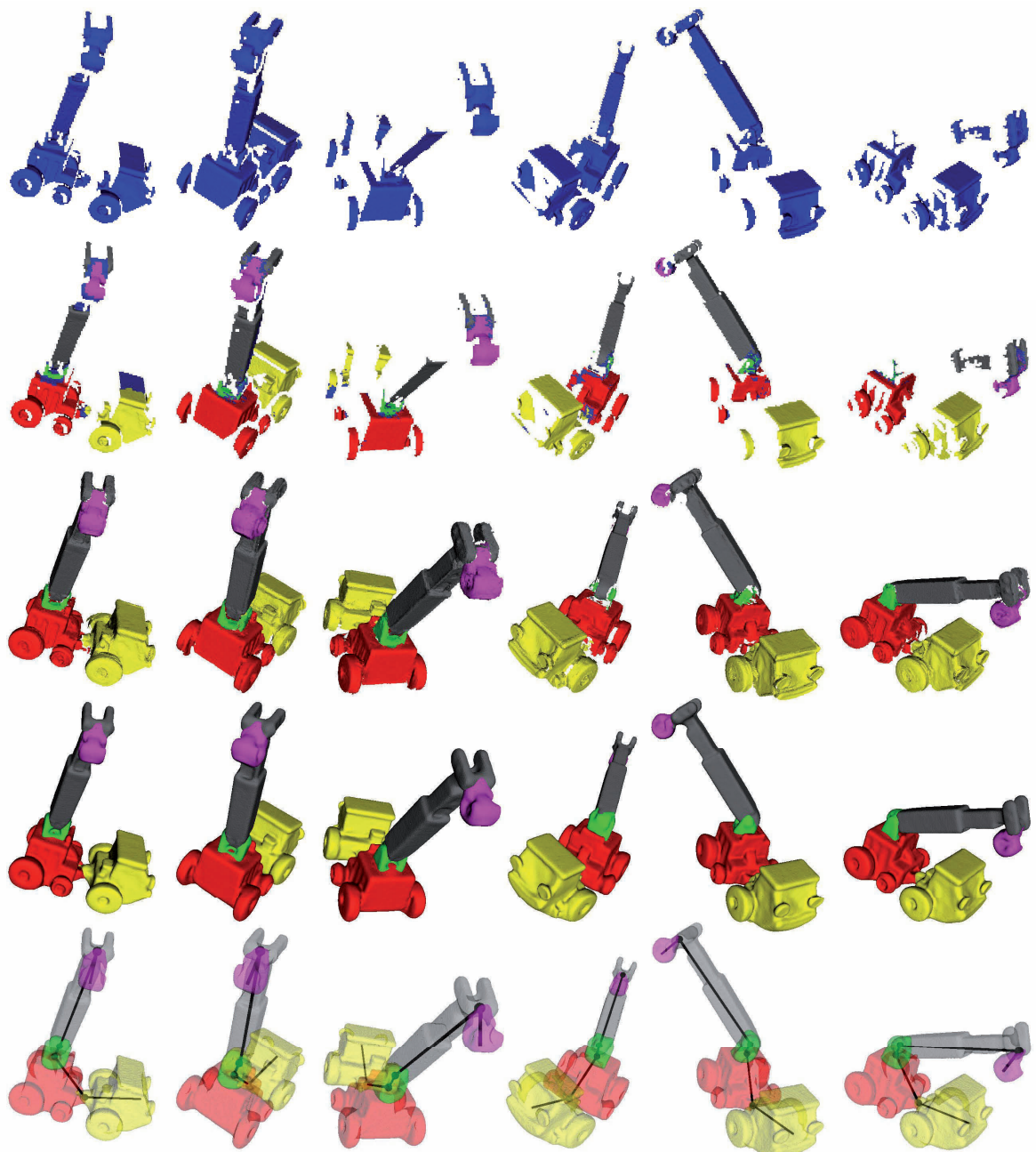


Figure 7: Scanning the dynamic real-world Tow-Truck model, consisting of 5 bones: **(Top row)** Some of the input depth frames obtained by a Vialux depth video camera. Note the different camera viewpoints and model poses. **(Second row)** Segmentation of the input frames into bones. Dark blue regions are undecided. **(Third row)** Accumulated skin geometry in input poses. Holes are present where the surface was occluded in all input frames. **(Fourth row)** Complete model in input poses after skin reconstruction. **(Bottom row)** Reconstructed skeletons.

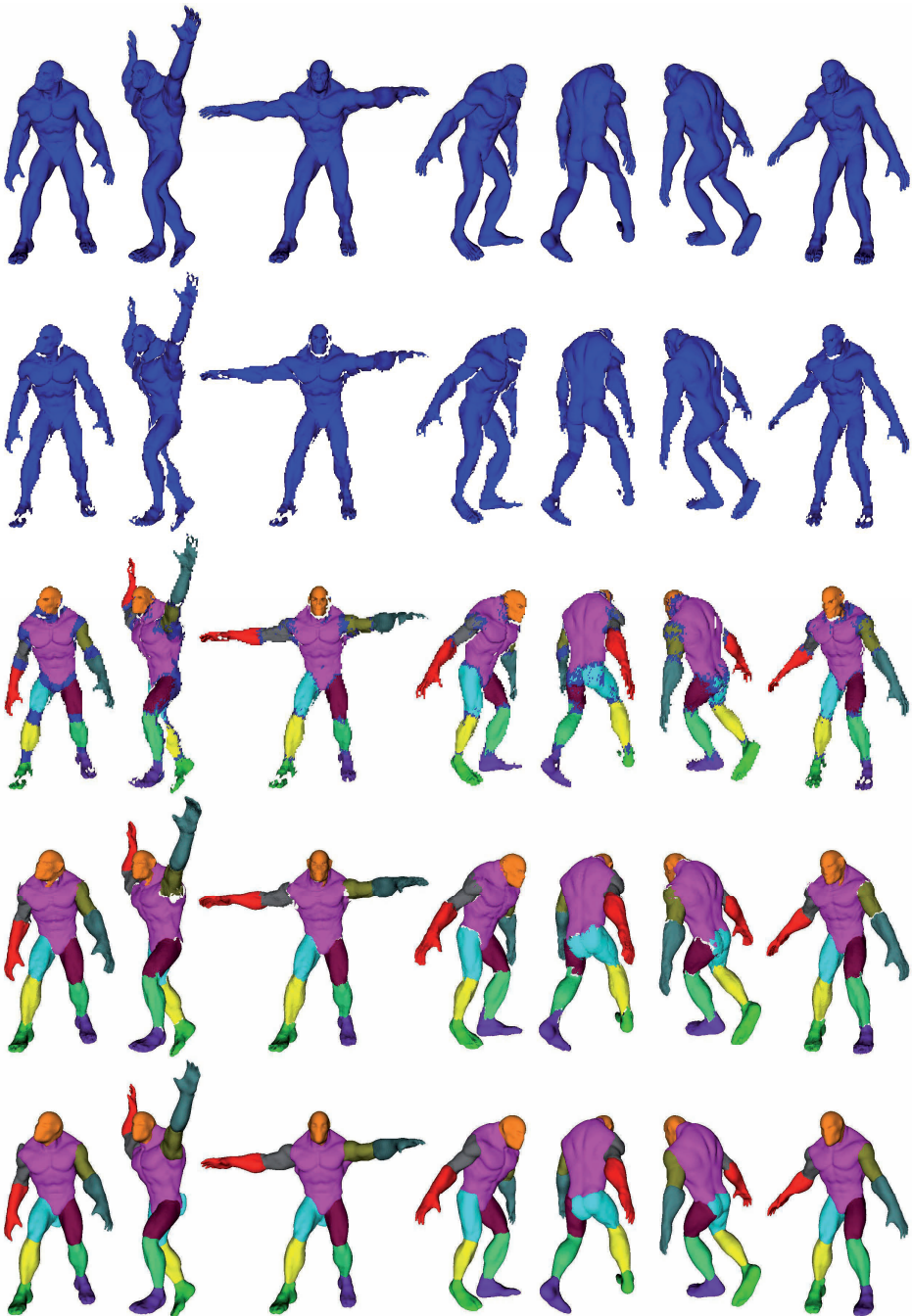


Figure 8: “Scanning” the synthetic deformable Monster model, consisting of 12 “bones”: **(Top row)** Frames from the synthetic animation sequence. **(Second row)** Input depth frames, as captured from the rendering z-buffer. **(Third row)** Segmentation of the input frames into bones. Dark blue regions are undecided. Note the incorrect classification of the rear end as part of the (light blue) right leg instead of the (purple) torso. **(Fourth row)** Accumulated skin geometry in input poses. Holes are present where the surface was occluded in all input frames. **(Bottom row)** Complete model in input poses after skin reconstruction.